University of New Hampshire
University of New Hampshire Scholars' Repository

Space Science Center | Institute for the Study of Earth, Oceans, and Space (EOS)

10-18-1996

Balloon-borne coded aperture telescope for arc-minute angular resolution at hard x-ray energies

Mark L. McConnell
University of New Hampshire - Main Campus, mark.mcconnell@unh.edu

V Boykin
University of New Hampshire - Main Campus

R M. Kippen
University of New Hampshire - Main Campus

K Larson
University of New Hampshire - Main Campus

John R. Macri
University of New Hampshire - Main Campus, John.Macri@unh.edu

See next page for additional authors

Follow this and additional works at: https://scholars.unh.edu/ssc

 Part of the Astrophysics and Astronomy Commons

Recommended Citation

Mark L. McConnell ; Valerie Boykin ; Richard M. Kippen ; Kipp Larson ; John R. Macri ; Michelle Mayer ; James M. Ryan ; Peter P. Altice, Jr. ; Michael L. Cherry ; Steven B. Ellison ; B. Price ; T. Gregory Guzik ; R. Lockwood ; M. B. Barakat ; K. Johnston ; N. Zotov and M. Elaasar "Balloon-borne coded aperture telescope for arc-minute angular resolution at hard x-ray energies", Proc. SPIE 2806, Gamma-Ray and Cosmic-Ray Detectors, Techniques, and Missions, 349 (October 18, 1996); doi:10.1117/12.253997; http://dx.doi.org/10.1117/12.253997

This Conference Proceeding is brought to you for free and open access by the Institute for the Study of Earth, Oceans, and Space (EOS) at University of New Hampshire Scholars' Repository. It has been accepted for inclusion in Space Science Center by an authorized administrator of University of New Hampshire Scholars' Repository. For more information, please contact nicole.hentz@unh.edu.

Balloon-borne coded aperture telescope for arc-minute angular resolution at hard x-ray energies

Rights
© (1996) COPYRIGHT SPIE--The International Society for Optical Engineering.

Authors
Mark L. McConnell, V Boykin, R M. Kippen, K Larson, John R. Macri, M Mayer, James M. Ryan, P P. Altice, M L. Cherry, S B. Ellison, B Price, T G. Guzik, R Lockwood, M B. Barakat, K Johnston, N Zotov, and M Elaasar

This conference proceeding is available at University of New Hampshire Scholars' Repository: https://scholars.unh.edu/ssc/104

A Balloon-Borne Coded Aperture Telescope for Arc-Minute Angular Resolution at Hard X-Ray Energies

M. McConnell, V. Boykin, R.M. Kippen, K. Larson, J. Macri, M. Mayer, J. Ryan
Space Science Center, University of New Hampshire, Durham, NH 03824

P. Altice, M.L. Cherry, S.B. Ellison, B. Price, T.G. Guzik, R. Lockwood
Dept. of Physics and Astronomy, Louisiana State University, Baton Rouge, LA 70803

M.B. Barakat, K. Johnston, N. Zotov, M. Elaasar
Dept. of Physics, Louisiana Tech University, Ruston, LA 71272

ABSTRACT

We are working on the development of a new balloon-borne telescope, MARGIE (Minute-of-Arc Resolution Gamma ray Imaging Experiment). It will be a coded aperture telescope designed to image hard X-rays (in various configurations) over the 20-600 keV range with an angular resolution approaching one arc minute. MARGIE will use one (or both) of two different detection plane technologies, each of which is capable of providing event locations with sub-mm accuracies. One such technology involves the use of Cadmium Zinc Telluride (CZT) strip detectors. We have successfully completed a series of laboratory measurements using a prototype CZT detector with 375 micron pitch. Spatial location accuracies of better than 375 microns have been demonstrated. A second type of detection plane would be based on CsI microfiber arrays coupled to a large area silicon CCD readout array. This approach would provide spatial resolutions comparable to that of the CZT prototype. In one possible configuration, the coded mask would be 0.5 mm thick tungsten, with 0.5 mm pixels at a distance of 1.5 m from the central detector, giving an angular resolution of 1 arc-minute and a fully coded field of view of 12 degrees. We review the capabilities of the MARGIE telescope and report on the status of our development efforts and our plans for a first balloon flight.

KEYWORDS: hard X-ray, gamma-ray, coded-aperture, imaging, Cadmium Zinc Telluride, CsI microfibers, charge-coupled devices, room-temperature semiconductors, astronomy

1. INTRODUCTION

At hard X-ray and γ-ray energies, photons cannot be easily focused. Directional information can be obtained at these energies by using the technique of coded aperture imaging. Coded aperture detectors have now been used on several balloon and spacecraft experiments, but the highest resolution coded aperture hard X-ray/γ-ray instrument to date has been the French-Soviet SIGMA experiment, with 13′ angular resolution.[1] The Minute of Arc Resolution Gamma-Ray Imaging Experiment (MARGIE) is designed to improve the coded aperture angular resolution down to a level of 2-6 arc-minutes. The key step in obtaining this improved angular resolution will be the use of two new technologies to provide the required high spatial-resolution photon detectors: room temperature cadmium zinc telluride (CdZnTe or CZT) semiconductor detectors for photon energies of 20-200 keV, and segmented scintillators coupled to bidirectional charge coupled device (CCD) readouts for photon energies of 50-600 keV.

Previous instruments[1,2,3,4,5] have all had mask pixel sizes on the order of ~1 cm. To obtain angular resolution of minutes of arc, however, submillimeter position resolution is required. Submillimeter (100-500 μm) resolution brings with it several issues which, though not crucial at centimeter scales, are very significant here. The detector position resolution must be $\lesssim$500 μm and the mask element size must be $\lesssim$1 mm. With such small detector pixels, "pixel crosstalk" then becomes a crucial issue at high energies; the very large number of pixels in the coded aperture pattern (641 × 643 for the first MARGIE flight) translates into a lengthy data processing effort with standard deconvolution techniques; and the large number of detector elements implies that low-power custom electronics are necessary. Our current effort has enabled us to identify these issues, demonstrate the required detector performance, and design an instrument capable of extending the coded aperture imaging technique into the minute-of-arc range. MARGIE will use new technology to push the coded aperture technique into this regime, and it will serve as a prototype for an eventual space instrument (e.g., a future MIDEX).

Downloaded From: http://proceedings.spiedigitallibrary.org/ on 11/25/2014 Terms of Use: http://spiedl.org/terms

2. THE MARGIE CONCEPT

A schematic of the initial flight configuration of the MARGIE instrument is shown in Fig. 1 (see also Table 1). The main detector components consist of the mask, the central detector (CZT and/or CsI-CCD), and the shields. We envision that the first balloon flight will be a 1-2 day continental US turnaround flight intended both as an initial engineering flight and to look at Northern Hemisphere sources with a wide field of view and good angular resolution. This configuration will use a high-resolution CZT detection plane and will concentrate on the energy range 20-200 keV.

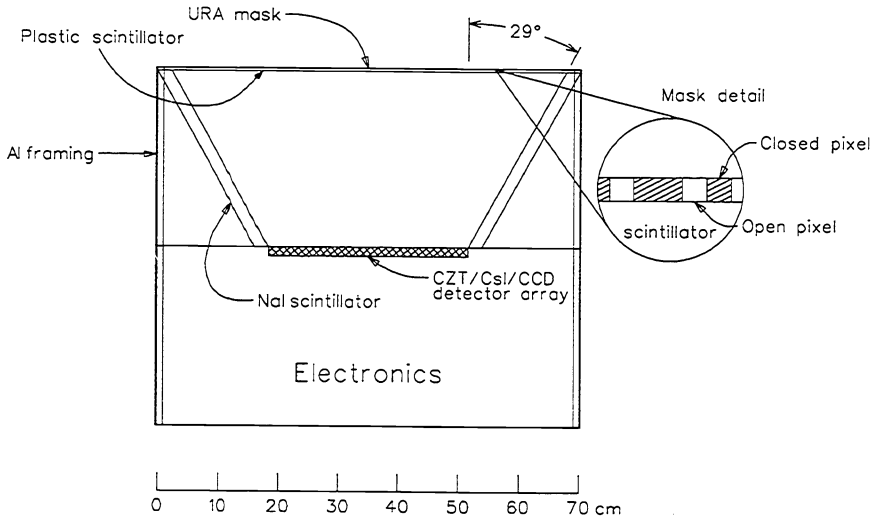

Figure 1 - A schematic diagram showing the basic elememts of the initial MARGIE payload.

The position-sensitive CZT γ-ray detector is an array of room temperature CZT strip detectors 1.5 mm thick. With a strip pitch of 375 μm, a spatial resolution of ~200 μm has been demonstrated during laboratory tests.[6,7,8,9] These detectors also exhibit clear photopeaks over a broad energy band from 30 to 662 keV (with FWHM < 10 keV and peak-to-valley ratio > 5:1 at 122 keV). An alternative MARGIE configuration, more suitable for higher energies, will use a 1 cm thick CsI microfiber array with 300 μm pixels coupled to a BiDirectional CCD with 50 μm spatial resolution and 30 μs timing resolution[10,11,12]. The individual CsI-CCD elements will be 512 × 512 pixel devices with $(2.6\ cm)^2$ active area operating over the energy range 50-600 keV. In either case, active side shields of 2 cm thick NaI(Tl) will be used to attenuate atmospheric photons and cosmic diffuse photons arriving from outside the telescope's field of view, and to serve as an active anticoincidence detector for charged cosmic ray particles. A thin plastic scintillator (~5 mm thick) will be placed below the tungsten mask as well, partly to serve as an active charged particle anticoincidence and partly for structural support.

For the initial MARGIE flight, the detector will be a 1090 cm^2 CZT array (with 760 cm^2 active area) at a distance of 30 cm from the coded mask. The mask itself, based on a 641 × 643 URA pattern, will be made of tungsten with a thickness of ~0.5 mm, providing adequate photon attenuation over the 20-200 keV energy range. Each mask element will be 0.5 mm × 0.5 mm in size. The resulting fully coded field of view will be 29° (half angle) with an angular resolution of 5.7 arc-minutes. The initial flight of this experiment will be a 24-48 hour flight from Ft. Sumner or Palestine. The scientific goals of this first flight will be to look at several northern hemisphere sources (e.g., the Crab, Cyg X-1, etc.) and to measure the emission along the galactic plane. The wide field-of-view and excellent angular resolution will also provide an opportunity to detect γ-ray bursts and to locate them with sub-arcminute resolution. Later balloon flights will incorporate a second detection plane consisting of an array of CsI-CCD detector modules. This array may either replace the CZT array or be added as a second detection layer. In either case, the MARGIE payload design is such that it will fit within the payload margins of a long duration balloon flight.

A higher-energy version of MARGIE, operating at energies up to 600 keV, could be achieved by replacing the initial mask with a thicker (5 mm) tungsten mask and using a CsI-CCD detector array. Although the thicker mask and thicker detector would limit the size of the field-of-view, high angular resolution would also be achieved by limiting the size of the

Downloaded From: http://proceedings.spiedigitallibrary.org/ on 11/25/2014 Terms of Use: http://spiedl.org/terms

field-of-view. In particular, with the CsI-CCD detection plane placed 1.5 m behind the mask, we would operate with a field-of-view of 6° and an angular resolution of 2.3 arc-minutes. This configuration would be ideal for mapping the distribution of 511 keV radiation along the galactic plane.

TABLE 1. MARGIE Parameters – Initial Flight Configuration

Detection plane (CdZnTe strip detectors)	Geometric Area	1090 cm^2
	Sensitive Area	760 cm^2
	Thickness	1.5 mm
	Strip Pitch	375 μm
	Spatial Resolution	~200 μm
	Timing Resolution	1 μs
Mask (graded W)	Pattern	643 x 641 URA
	Element Size	0.5 x 0.5 mm
	Thickness	~ 0.5 mm
	Distance from Detector	30 cm
Imaging	Field-of-View (FoV)	29° (half-width)
	Angular Resolution	5.7′
Spectral	Energy Range	20-200 keV
	Energy Resolution	<8 keV FWHM @ 60 keV
		<10 keV FWHM @ 122 keV
	Sensitivity (3 σ)	46 mCrab (1hour) @ 30-50 keV
		210 mCrab (1 hour) @ 150-200 keV

3. THE IMAGING SYSTEM

3.1 Design Considerations

The coded aperture (or "multi-pinhole") technique works by allowing an absorbing mask to cast a shadow pattern on a position-sensitive detection plane.[13,14] With a proper choice of mask pattern to minimize artifacts from the imaging process, the encoded pattern can then be processed to reproduce an image of the sky. The MARGIE mask design will be based on the uniformly redundant array (URA) patterns[15] that have been successfully used in several previous experiments. A common approach is to fabricate a mask using a 2×2 mosaic of the basic $n \times m$ URA pattern. In this configuration, the detection plane is the same size as the basic URA pattern. This design insures that no ambiguities are introduced into the imaging process.

Several interrelated parameters must be considered in designing an imaging system. The angular resolution corresponds to the angular size of a mask element as seen from the detection plane, and so is dictated by the mask element size and the separation of the mask from the detector. In order to achieve this level of angular resolution, however, the detection plane must be able to resolve the individual mask elements in the projected pattern; i.e., the detector must be able to locate events with an accuracy no larger than the mask element size. The exact ratio between detector spatial resolution and mask element size has an important effect on the S/N in the reproduced image.[16,17] For a fixed element size, improved spatial resolution results in an improvement in the imaging S/N. One can think of this as an improvement in the ability of the detection plane to define the shadow produced by the mask. Any technology (such as those used here) which improves the detector plane spatial resolution can therefore lead to an improvement in telescope sensitivity. It has also been shown[17] that improved performance (in terms of a more uniform response within the FoV) results from non-integral ratios of mask pixel size to

Downloaded From: http://proceedings.spiedigitallibrary.org/ on 11/25/2014 Terms of Use: http://spiedl.org/terms

detector resolution. These considerations lead to the constraint that the mask element size should be at least ~1.5 times larger than the detector spatial resolution.

The FoV is determined principally by the geometric area of the detector and the mask-detector separation d. In particular, the half-width of the FoV can be expressed as

$$\theta \sim \tan^{-1} \frac{\sqrt{NM}}{2} \frac{w_m}{d} \tag{1}$$

where N and M are the indices of the URA pattern and w_m is the mask element width. Several factors will, however, act to impose limits on the maximum allowable size of the FoV. Most important of these are the mask and detector element geometry.

The mask element geometry is defined by the mask thickness and the mask element size (or width). The mask thickness must be sufficient to attenuate photons (hence, modulate the incident flux) in the desired energy range. On the other hand, the thickness of the mask must be limited so as to maintain uniformity of mask transmission for off-axis sources. (For thick masks, the resulting shadow may become distorted for sources at large off-axis angles.) In general, the greater the FoV, the smaller the required thickness-to-width ratio.

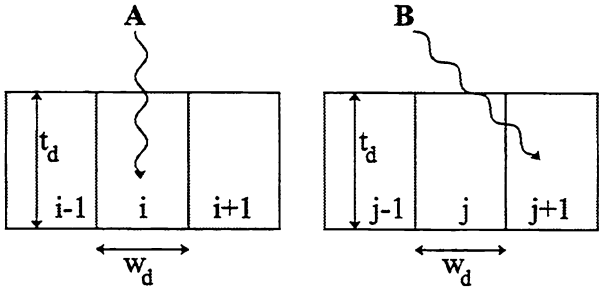

Figure 2. Pixel crosstalk.

As with the mask element geometry, the detector element geometry is defined by the detector thickness and the detector element size (or, equivalently, the detector spatial resolution). An important consideration is the lateral distance traveled by a photon in the detector material before it interacts. This will depend not only on the angle of incidence of the photon, but also on its energy (i.e., its mean free path in the detector material). The concern is that the photon may strike the detector surface at a point (in x,y) which is greater than one resolution element away from the interaction location. Since we are interested in mapping out the distribution of photons across some particular (x,y) plane (usually the top surface of the detector), the event would be registered with some significant error in its location. This "crosstalk" leads to a degradation of the imaging performance (i.e., a smearing of the point spread function). This (often neglected) crosstalk effect can be minimized at a given energy by limiting the FoV or by limiting the detector thickness. Since the detector thickness is usually dictated by the energy range of the instrument, this really implies a limit on the FoV. Because the pathlength increases with energy, this effect is more pronounced at higher energies. Fig. 2 illustrates this effect. Here photon A is vertically incident, arrives at the top surface of pixel i, and is detected in pixel i. Photon B, however, comes from a wide angle, arrives at pixel j, and is detected in pixel j+1. If the photon is to be detected with good efficiency and this "crosstalk" effect is to be kept small, then the photon attenuation length λ (E) and the zenith angle θ combine to put constraints on the detector pixel size w_d and detector thickness t_d. Let us define some maximum possible photon pathlength (η), which can be expressed as some factor (f) times the photon attenuation length,

$$\eta(E) = f\ \lambda(E) \tag{2}$$

This defines, for a given maximum energy (E_{max}), the required thickness of the detector,

$$\eta(E_{max}) = f\ \lambda(E_{max}) \sim t_d \tag{3}$$

We see that the parameter f represents the thickness of the CZT in terms of the number of photon attenuation lengths at E_{max}. A detection efficiency of 40% corresponds to a value of 0.5 for f. Based on this constraint, a CZT detector thickness of 1.5 mm implies a maximum operational energy E_{max} ~ 200 keV. For off-axis viewing ($\theta > 0°$), we have the following additional constraints on both the detector thickness and the detector pixel size (c.f., Fig. 2),

$$f\ \lambda\ \cos\theta \leq t_d \qquad\qquad f\ \lambda\ \sin\theta \leq w_d \tag{4}$$

Downloaded From: http://proceedings.spiedigitallibrary.org/ on 11/25/2014 Terms of Use: http://spiedl.org/terms

These constraints also imply a maximum opening angle (or maximum FoV) which is a function of the energy. In particular, from eqn. (4),

$$\theta_{max}(E) \leq \sin^{-1}\left(\frac{w_d}{f\ \lambda(E)}\right) \tag{5}$$

This angle decreases with energy such that, at the maximum energy, we have, from eqns. (3) and (4),

$$\theta_{max}(E_{max}) \leq \sin^{-1}\left(\frac{w_d}{t_d}\right) \tag{6}$$

When detector plane pixel sizes decrease to the ~1 mm scale or less these considerations become significant. In the case of sufficiently large incident angles that violate Eqs. 4 and 5, the crosstalk from one pixel to the adjacent pixel can cause a serious degradation in both the imaging characteristics and the source sensitivity. Although these criteria do not represent strict limitations, it should be noted that any proposed coded aperture instrument design should not significantly violate these criteria.

One approach in dealing with these constraints is to provide additional information on the depth of the interaction site within the detection plane. This permits the differentiation of "deep" interactions (where the measured position may be displaced from the entrance point) from "shallow" interactions near the top of the detector (where the crosstalk is small and the measured interaction point is a good measure of the actual entrance location). The MARGIE CZT will have the capability to measure the depth of the interaction by measuring the relative anode-cathode signal amplitudes and the width of the charge distribution, and so will be able to discriminate between shallow and deep events in the detector.[9]

For its initial flight, MARGIE is intended to be a wide-FoV, high angular resolution imaging telescope characterized by the parameters in Table 1. At 50 keV, where the mean free path (λ) in CZT is 0.16 mm, Eq. 5 implies that $\theta_{max} = 29°$. (We chose 50 keV in this case because this is near the peak of the γ–ray burst fluence.) At 200 keV, where Eq. 6 applies, the FoV is constrained by the detector parameters; here $\theta_{max} = 14°$. Analysis of the data at higher energies requires the incorporation of information on the interaction depth within the CZT. For later balloon flights, we envision a mask element size of 1 mm at a distance of 1.5 m, corresponding to a FoV with half-angle 6° and an angular resolution of 2.3′. Both of these configurations are significant improvements compared to previous instruments.

3.2 Mask Fabrication

We have developed and tested the procedures for producing large coded aperture tungsten masks using relatively straightforward photolithographic etching techniques. We start with rolled tungsten sheet that has been cleaned to remove any oxides. Cutting the tungsten is undesirable because the required heating leads to oxidation. A mask pattern is produced which provides for the "edge allowances" required to produce the proper shaped holes. The mask pattern is transferred from CAD to a silver-based mylar acetate film using a high resolution (16,000 dpi) laser printer. Photoresist is rolled onto the tungsten, and two acetate masks are applied to the front and back of the tungsten using double-sided tape. The two masks are aligned using markers on the overlapping edges. The tungsten-acetate sandwich is then illuminated with UV light which photoexcites the resist through the clear holes in the mask. The acetate film is removed, the resist is developed in soda ash to harden the unexposed photoresist, and the excited polymer photoresist is washed away. The piece is then etched in an acid "soup" at a predetermined rate and temperature, rinsed with water, and stripped of the photoresist. An X-ray image of a prototype mask, taken with 40 - 50 keV X-rays from a dental X-ray machine using a CsI microfiber array and CCD camera is shown in Fig. 3.

Energetic photons and cosmic ray particles striking the tungsten will produce fluorescence photons at an energy just below that of the tungsten K-edge. In order to attenuate the tungsten fluorescence photons, a graded mask will be used. We are investigating various options for the grading material(s) and thicknesses. The choice will be dictated by the physical properties, ease of handling, cost of the material, and the imaging properties. Tin and silver foils, for example, are both potentially useful. A silver or tin mask layer can be etched, aligned (using the same procedure as for the acetate masks), and glued to the back of the tungsten in a graded sandwich to produce the final MARGIE mask. (The silver and tin etching

Downloaded From: http://proceedings.spiedigitallibrary.org/ on 11/25/2014 Terms of Use: http://spiedl.org/terms

procedures are the same as for the tungsten except that a different acid "soup" composition is required, the complication of the "edge allowances" needed to etch the thick tungsten layer is eliminated and the difficulty of working with brittle tungsten is removed.) Our initial sensitivity estimates incorporate a W-Ag mask. A thin layer of plastic scintillator is placed below the mask for mechanical support and to provide a means of rejecting charged particles.

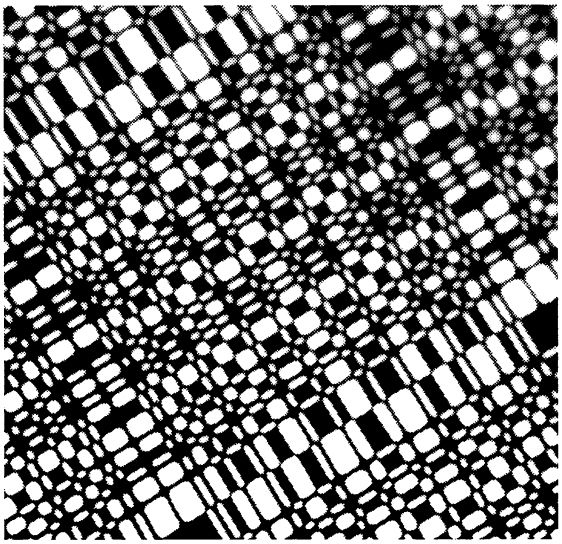

Figure 3. X-ray image of an etched tungsten mask obtained with a 1 mm thick CsI microfiber array and a CCD camera. The mask is a 71 x 73 URA pattern with 0.5 mm thickness and 0.5 mm minimum pixel dimensions.

4. DETECTION PLANE TECHNOLOGIES

4.1 Cadmium Zinc Telluride

The central detector plane for the initial MARGIE instrument will be composed of a closely-packed array of imaging CdZnTe (CZT) strip detector modules. CZT is a compound semiconductor material increasingly employed in room temperature X- and γ-radiation detection applications. Detectors constructed of CZT provide high stopping power in compact packages operating without the need for cryogenic cooling.[18]

Fig. 4 is a photograph of the prototype strip detector manufactured by DIGIRAD of San Diego, CA . It consists of a monolithic $Cd_{0.9}Zn_{0.1}Te$ substrate measuring 28 × 28 mm by 1.5 mm thick with 64 gold strip contacts and 2 guard strips on each surface. The strip pitch, which corresponds to the effective pixel size, is 375 μm in both dimensions, with an effective imaging area of 576 mm^2. The CdZnTe array is mounted in a printed circuit board carrier with contacts to all strips in a standard pin grid array pattern for safe handling and testing. An 11 × 12 array of 132 modules will be used to define an image plane with 760 cm^2 active area for MARGIE.

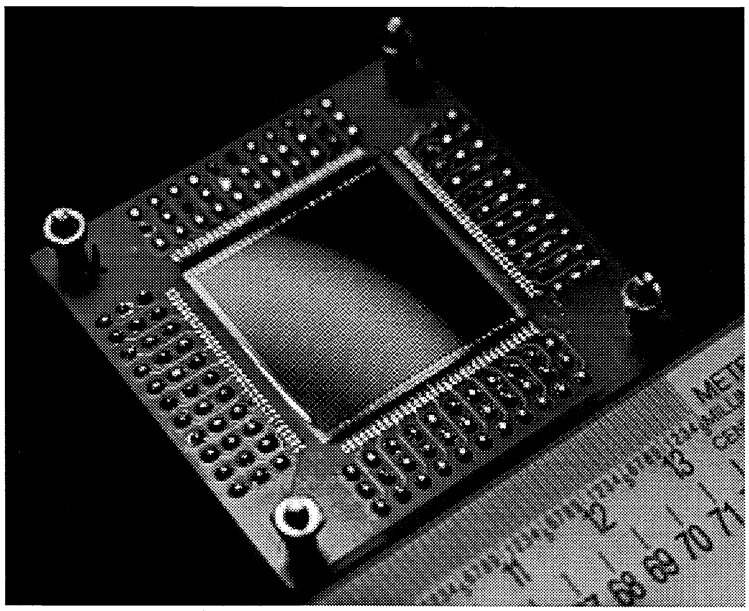

Figure 4. Photo of UNH prototype CZT strip detector.

Fig. 5 shows a schematic diagram of a small portion of the strip detector to illustrate the principle for measuring the photon interaction site and the photon energy deposit. An incident gamma-ray photon interacts at a point within the strip detector generating an ionization charge region whose extent is determined by scattering and fluorescence processes. Calculations and measurements with CZT pixel detectors have determined the extent of this ionization site to be ~200 μm.[19] Charge signals in proportion to the deposited energy and related to the transport of these ionization charges (electrons and holes) are detected on each surface on the contact strips near the photon interaction site. The electrons, transported along the Z dimension by the bias field, are collected on the nearest anode strips. Except for interactions occurring at the cathode surface, the holes, with relatively poor charge transport properties, are not fully collected during the amplifier's integration time.[20] Rather, signals are induced on the individual cathode strips in relation to the distance from the strip and the

Downloaded From: http://proceedings.spiedigitallibrary.org/ on 11/25/2014 Terms of Use: http://spiedl.org/terms

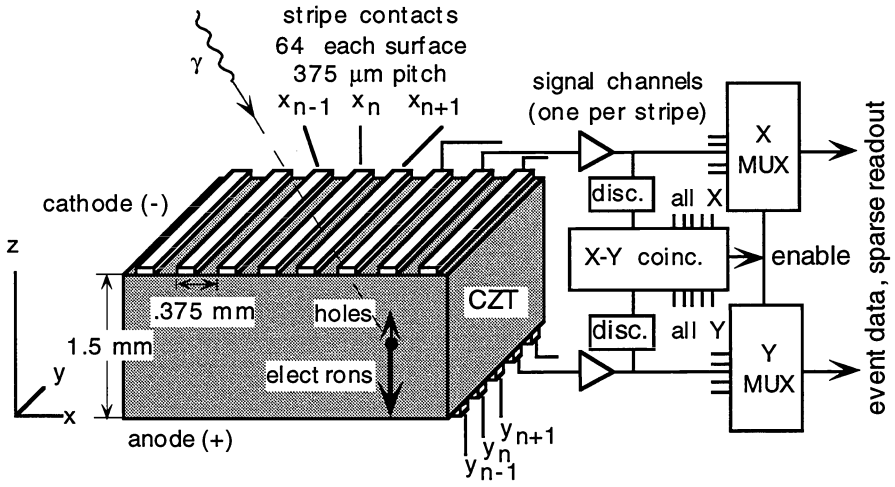

Figure 5. Strip detector operating principles. The event location "pixel" is defined by the intersecting coordinates of coincident x-y signals. The energy deposit is determined from the amplitude of the anode signal .

amount of hole transport that takes place during the amplifier's integration time. Our measurements show that the size of this hole signal relative to the electron signal depends on the depth of the photon's interaction.

The strip IDs and pulse heights of coincident X-Y signals define the photon interaction location in the X and Y dimensions. The Z dimension is determined for each event by measuring the relative X and Y pulse heights. A photon interaction site far from the cathode surface results in relatively lower cathode pulse height than is observed when the interaction site is close to the cathode. As with pixel detectors, pulse height analysis of the anode signals provides the optimum energy measurement.[9]

The first tests of the prototype CZT detector were made using conventional laboratory electronics to characterize the response and evaluate the performance of these detectors.[6,7,8,9] The small number of available electronic channels limited these tests to small regions of the prototype detectors. The results, however, clearly demonstrated the potential of CZT strip detectors to function as excellent sub-millimeter resolution imaging spectrometers in the proposed energy range. As an example of the CZT characteristics, Fig. 6 shows the spectrum of ^{57}Co (122 keV) obtained from a single pixel element within the strip detector.

MARGIE's strip detectors will be packaged according to a proprietary Digirad design in rugged ceramic carriers permitting assembly of a closely-packed array of strip detector modules with at least 70% active imaging area. Continued development of alternative packaging concepts under consideration by Digirad may lead to strip detector modules with a significantly higher fraction of active imaging area. CMOS and chip-on-board technologies provide the capability to produce the strip detector signal processing circuitry within the area beneath each of MARGIE's CZT strip detectors.

The 64 × 64 contact strip pattern of each CZT module defines a square 4096 pixel imaging area with 128 electronic

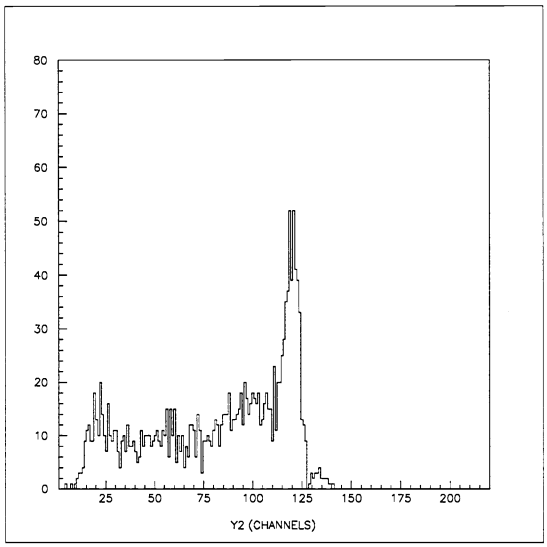

Figure 6. Spectrum of ^{57}Co (122 keV) as measured from a single 375 μm pixel.

Downloaded From: http://proceedings.spiedigitallibrary.org/ on 11/25/2014 Terms of Use: http://spiedl.org/terms

channels. Applying the strip detector principle minimizes the number of required signal channels, provides good energy resolution, permits event location in 3 dimensions, and permits the development of large area imagers with event-triggered readout electronics. Event-triggered processing permits precise timing of the detection (~1 μs) as well as the determination of coincidence and anti-coincidence or relative timing with external events. This is important in high background environments. The MARGIE CZT dimensions are chosen to optimize the energy resolution[21] and the position resolution[22] and to satisfy the imaging constraints in Sec. 3.1. The choice of an orthogonal strip geometry rather than a pixel geometry is made to facilitate event-triggered readout and permit the interaction depth determination as well as to minimize the number of electronic channels and the associated power.

4.2 CsI Microfiber Arrays

The 1.5 mm thickness and the 375 μm strip pitch of the MARGIE CZT are optimized for both energy and spatial resolution.[22] The CZT thickness limits us, however, to a maximum energy of ~200 keV. Thicker CZT detectors could be used in order to extend the energy range upward, but then the CZT cost would also increase. We are therefore investigating an alternate approach to achieve arc-minute angular resolution at energies upwards of 511 keV. This approach is based on the use of high resolution segmented scintillators. In particular, we have been exploring the use of fine-grained arrays of "light pipes" of CsI scintillator viewed by silicon CCDs. Cherry et al.[10] and Nagarkar et al.[23] have described the possibilities of growing very high resolution CsI microfiber arrays (Fig. 7). We have demonstrated light yield comparable to that of bulk CsI (>30 photons/keV) with a position resolution <100 μm. As an example of the capability of this technology, Fig. 3 shows an image of a tungsten mask (with 0.5 mm pixels) taken with a 1 mm thick CsI scintillator array produced at Radiation Monitoring Devices, Inc (RMD). The source is 40-50 keV X-rays from a dental X-ray machine; the scintillation light is viewed by a CCD.

At the present time, the ability to grow CsI arrays with well-defined columnar structures of ~100 μm diameter is limited to thicknesses of a few mm. Thicknesses of 1 cm or so, as would be required to reach energies up to 600 keV, could be achieved by limiting the spatial resolution to ~300 μm and forming the CsI scintillator columns in a metal matrix using a vacuum injection technique developed by RMD. A honeycomb metal mesh matrix is the basic structure. Such materials are used in aircraft wings and other applications requiring light weight and strength, and can be fabricated inexpensively in large areas with cell diameters as small as 300 μm and fill factors >85%. The thin metal walls between cells are opaque, and therefore eliminate the spreading of the optical light measured in a standard thick single scintillator and (to a lesser extent) in our microfiber arrays. A high atomic number metal limits the energy spread of the primary X-ray interaction due to Compton scattering and high energy photoelectrons. CsI is a suitable material for vacuum injection at reasonable temperatures. The scintillator material is injected into the mold in liquid form and then allowed to solidify into single crystals. Prototypes have now been produced with thicknesses up to 2 cm, and are currently being tested.

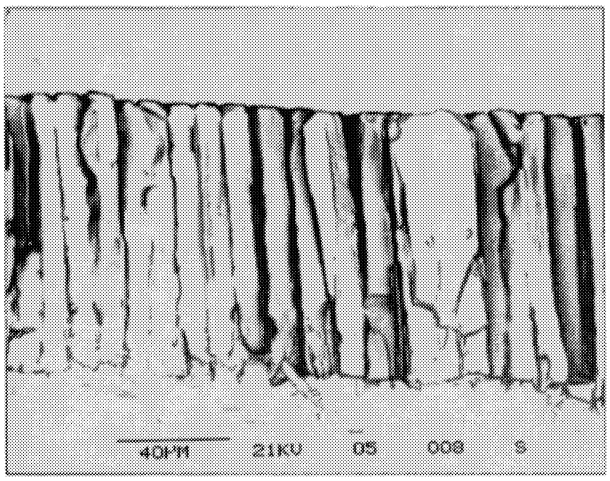

Figure. 7. Scanning electron microscope picture of a 100 μm thick CsI(Tl) fiber layer deposited at RMD.

CsI (Tl) is reasonably transparent to its peak emission at 550 nm, and a silicon CCD can be used to detect light with ~35% quantum efficiency. CCDs are, for many applications, nearly ideal light detectors. They are reliable, and provide excellent position resolution with low noise. For our application, however, a standard CCD is slow – CCDs typically operate at no better than video rates (20 - 30 frames/s). This is too slow to operate with an active charged particle anticoincidence shield. (In the case of MARGIE, a cosmic ray proton will strike the shields or the mask and potentially generate a bremsstrahlung photon approximately every 250 μs. With 30 μs CCD timing, individual cosmic ray shield hits can be flagged and then removed during the analysis.) We have therefore developed a new CCD readout architecture providing 30 μs time resolution and lower noise performance. This BiDirectional Fast Timing CCD[11,12] will

Downloaded From: http://proceedings.spiedigitallibrary.org/ on 11/25/2014 Terms of Use: http://spiedl.org/terms

also have applications to medical imaging, inspection on moving assembly lines, reconnaisance from fast moving vehicles and aircraft, and CCD spectroscopy (where sufficient timing resolution is necessary to insure only one photon "hit" per pixel per readout).

5. INSTRUMENT BACKGROUND AND SOURCE SENSITIVITY

The sensitivity of MARGIE to astronomical sources depends not only on the efficiency of the detection plane, but also on the level of background encountered at float altitude. An accurate estimate of the in-flight background is therefore required in order to obtain meaningful sensitivity estimates. The primary sources of instrumental background at balloon altitudes include:

Aperture photon flux — This includes all non-source photons that enter through the forward aperture. The principal contributions come from the Earth's atmosphere and from the cosmic diffuse flux. In a coded-mask telescope, half of these photons are stopped (or scattered) by the mask.

Shield photon leakage — This includes photons that pass through the anticoincidence shield and are detected in the central detector without any shield signal. As with the aperture flux, the principal contributions come from the Earth's atmosphere and the cosmic diffuse flux.

Atmospheric neutrons — Neutron interactions within the experiment contribute to the background counting rate in at least two ways. Thermal neutron capture and inelastic collisions often give rise to photons in our energy range. In both cases, events in the 20–200 keV range can take place within the central detector. The inelastic neutron scatters are particularly troublesome. Typically, they excite a nucleus into a high-energy state or the continuum and the nucleus de-excites by emitting several photons. This makes it important to have an active shield. A passive shield must be very thick in order to stop all the secondary photons generated in the shield itself, whereas an active shield must only detect one secondary.

Charged particles — Charged particles (both electrons and protons) passing through the central detector produce large signals. These can be eliminated with active scintillators to detect (and reject) minimum ionizing particles.

Effects of the coded mask — The presence of the coded mask can influence the background rate in several ways. Background photons are generated in the mask by charged particles and high-energy photons. Photons that might otherwise miss the detector may be scattered towards the detector by the mask.

We have estimated the background counting rate using a Monte Carlo simulation using the CERN-GEANT software code. We have considered only the effects of the atmospheric flux and the cosmic diffuse photon flux at a depth of 3.5 g/cm^2 over Palestine, TX.[24] These are expected to be the dominant background components below 200 keV. [5,24,25,26] The results for the predicted background shown in Fig. 8 are based on the MARGIE design (Table 1) which incorporates an active 2 cm NaI shield surrounding the CZT detection plane and extending up to the mask 30 cm away. The mask itself was modeled as tungsten backed by a thin layer of silver, so we have included the effects of mask transmission, K-edge fluorescence, etc. The simulations clearly show that the dominant contribution to the background counting rate is the flux entering through the open aperture. Although there remains some evidence of the tungsten fluorescence lines near 60 keV, the level of these lines has been substantially reduced by the addition of the silver backing to the mask. (Note that tin would also work just as well as a grading material for the mask.)

In order to estimate the source sensitivity, we have simulated an E^{-2} Crab spectrum with an atmospheric attenuation corresponding to a zenith angle of 20° at an atmospheric depth of 3.5 g/cm^2. These data, when combined with the predicted background rates shown in Fig. 8, lead to the continuum sensitivity estimates shown in Fig. 9. For a 1-hour exposure, we expect a 30-50 keV 3σ sensitivity of 46 mCrab (a 65σ measurement on the Crab itself). This decreases to roughly 210 mCrab (a 15σ measurement on the Crab itself) in the 150-200 keV range. For a 10-hour observation, the sensitivity numbers become 15 mCrab and 70 mCrab, respectively.

Downloaded From: http://proceedings.spiedigitallibrary.org/ on 11/25/2014 Terms of Use: http://spiedl.org/terms

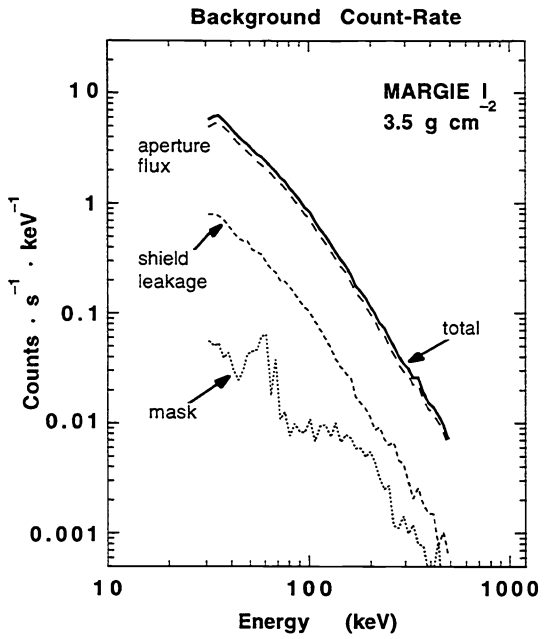

Figure 8. Expected background, based on Monte Carlo simulations of the intial MARGIE payload configuration.

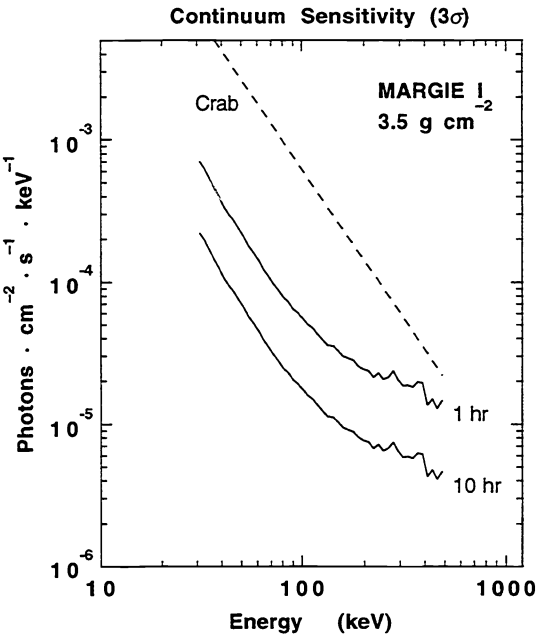

Figure 9. Instrument sensitivity. Dashed line is the continuum Crab spectrum. Solid lines are calculated MARGIE sensitivities for one and ten hour observations.

6. DATA ANALYSIS ISSUES

The analysis of MARGIE data is straightforward and will, in general, be based on past experience with coded aperture telescopes.[14] The large number of image elements (~4 × 10^5) in the basic MARGIE URA pattern does, however, impose a sizeable processing requirement. The standard deconvolution of coded mask data, involving a correlation between the detection plane response and a post-processing function (which is based on the mask pattern), can be extremely time consuming for such large images. For example, on an Alpha 3000 workstation the standard deconvolution of a 643 × 641 detector array requires roughly 19 hours of CPU time. Given that a typical image accumulation time is expected to be well under one minute (depending on the degree of payload stabilization), this would suggest that the data processing might take several orders of magnitude longer than the data collection itself. More rapid processing of the image data is clearly desirable. The processing time can be improved by suitable modifications to the standard deconvolution algorithm.[27]. A considerable increase in processing speed can also be achieved using an FFT algorithm. Although some authors[14,15] warn of the possibility of the FFT introducing unwanted noise into the reconstructed image, the speed advantage of the FFT makes this a potentially attractive option. For example, the image processing time for the same 643 × 641 detector array can be reduced to ~80 seconds using an FFT approach. In Figure 10, we show an image deconvolved using an FFT algorithm. (In this case, the data were obtained using a high spatial resolution amorphous silicon detector array in conjunction with the test mask shown in Figure 3.)

The number of independent image reconstructions (hence, the total data processing time) that will be required depends directly on the number of aspect bins (i.e., the number of independent pointing directions) used in the analysis. It also will depend on the number of independent energy bins. The number of aspect bins will be determined by the level of payload stabilization. A level of stabilization that is comparable to the image element size (5-10 arc-minutes) will lead to the minimum number of aspect bins. Clearly, this approach to the image reconstruction will require data processing times that are heavily influenced by the level of payload stabilization.

Downloaded From: http://proceedings.spiedigitallibrary.org/ on 11/25/2014 Terms of Use: http://spiedl.org/terms

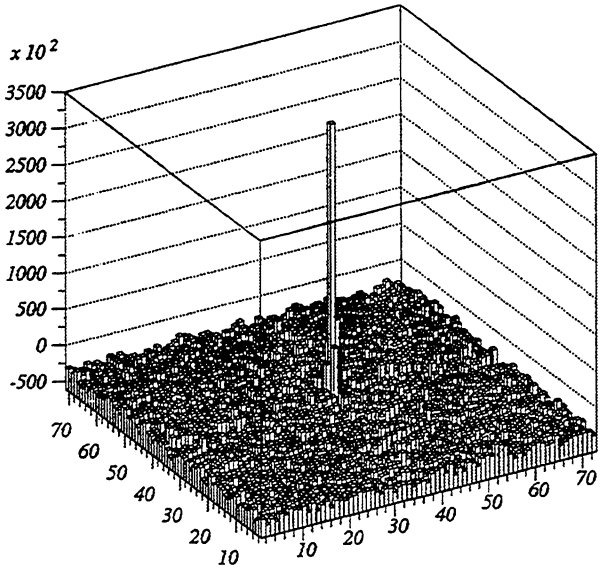

Figure 10. Reconstructed image based on test results with optical light beam illuminating 71 x 73 test mask. Signal is observed with 8" x 11" (127 μm pixel pitch) amorphous silicon detector array from Xerox Palo Alto.

Partly motivated by a desire to simplify the active pointing requirements, we have investigated an image reconstruction that involves the backprojection of each individual event through the mask and onto the sky. In this approach, each event is projected through each open element in the mask to the corresponding sky bins. An accumulation of a large number of events in this manner leads to the reconstruction of a sky image. (This method is similar to the tagged URA approach of Fenimore.[28]) Since each event is tagged with its own instantaneous payload pointing direction (aspect) and energy, the backprojection needs to be performed only once. Computational requirements may therefore be relatively small. With this approach, the requirements imposed on the payload stabilization are minimal. The critical requirement here is that each event be associated with some well-defined pointing direction.

Several other factors must also be considered in the analysis of MARGIE data. For example, we must make provisions for the correction of nonuniformities (in terms of both background and detection efficiency) across the detection plane. Both can lead to undesirable noise in the reproduced image. Several experiments (e.g., DGT, SIGMA, EXITE) have now demonstrated that flat-fielding of the detection plane distributions can be achieved.[5,29,30] Nonuniformities in detection plane sensitivity will be thoroughly studied during pre-flight calibration measurements. Another important issue is that the CZT array will be made up of individual CZT modules, each with some associated deadspace (~30%) due to the electronic contacts for the CZT strips. The (periodic) deadspace will lead to a non-ideal point spread function.[31] We are investigating various means for mitigating the effects of these dead areas. These include filling in the dead areas of the detector response with some average value based on the surrounding detector area, and post-image deconvolution based on the calibrated point spread function.

7. FUTURE PLANS

The MARGIE project represents a multi-faceted approach towards achieving high angular resolution astronomical imaging at hard X-ray and soft gamma-ray energies. Pending funding approval, we plan to perform the first flight of MARGIE in 1999, using the configuration outlined in Table 1. Subsequent balloon flights will provide the opportunity to further refine and develop the detection plane technologies we have outlined here while providing the capability to carry out useful scientific investigations.

8. ACKNOWLEDGEMENTS

This work has been supported by NASA Astrophysics at LSU and UNH, and by funding from NASA EPSCoR and the Louisiana Board of Regents at LA Tech.

9. REFERENCES

1. J. Paul et al., "Sigma – The Hard X-Ray and Soft Gama-Ray Telescope on Board the Granat Space Observatory", Adv. Space Research, 11, 289-302, 1991.

2. W.E. Althouse et al., "A Balloon-Borne Imaging Gamma-Ray Telescope", Proc. 19th Intl. Cosmic Ray Conf. (LaJolla), Vol. 3, 299-302, 1995.

3. S.M. Schindler et al., "GRIP-2: A Sensitive Balloon-Borne Gamma-Ray Telescope", submitted to Nucl. Instrum. and Meth., 1996.

4. J.E. Grindlay et al., "The Energetic X-Ray Imaging Telescope Experiment (EXITE)", IEEE Trans. Nucl. Sci, 33, 75-754 (1986).

Downloaded From: http://proceedings.spiedigitallibrary.org/ on 11/25/2014 Terms of Use: http://spiedl.org/terms

5. P.P. Dunphy et al., "A Balloon-Borne Coded Aperture Telescope for Low-Energy Gamma-Ray Astronomy", Nucl. Instrum. Meth., A274, 362–379, 1989.

6. J.M. Ryan et al., "Large Area Sub-Millimeter Resolution Cd Zn Te Strip Detector for Astronomy", SPIE Conf. Proc. 2518, 292 (1995).

7. J.R. Macri et al., "Large Area Sub-Millimeter Resolution CdZnTe Strip Detector for Astronomy", Proc. 9th Intl. Workshop on Room Temperature Semiconductor X and γ Ray Detectors, Associated Electronics and Applications, Grenoble, to be published in Nucl. Instrum. Meth.(1995a).

8. J.R. Macri et al., "Development of an Orthogonal-Strip CdZnTe Gamma Radiation Imaging Spectrometer", IEEE Trans. Nucl. Sci., 43, 1458-1462, 1996.

9. J.R. Macri et al., "Progress in the Development of Large Area Sub-millimeter CdZnTe Strip Detectors", to be published in SPIE Conf. Proc., 2859, 1996.

10. M.L. Cherry et al., "A New Balloon-Borne Detector for High Angular Resolution Hard X-Ray Astronomy", Proc. 24th Intl. Cosmic Ray Conference (Rome), 2, 45-48, 1995.

11. M.L. Cherry et al., "Charge Coupled Devices with Fast Timing for Space Physics Research", MASS/Airwatch Workshop Report (Huntsville), 259, 1995.

12. M.L. Cherry et al., "Charge-Coupled Devices with Fast Timing for Astrophysics and Space Physics Research", to be published in SPIE Conf. Proc., 2806, 1996.

13. E. Caroli et al., "Coded-Aperture Imaging in X-Ray and Gamma-Ray Astronomy", Space Science Rev., 45, 349-403, 1987.

14. G.K. Skinner et al., "Techniques for the Analysis of Data from Coded-Mask X-Ray Telescopes", Astr. & Space Sci., 136, 337-349, 1987.

15. E.E. Fenimore and T.M. Cannon, "Uniformly Redundant Arrays: Digital Reconstruction Methods", Applied Optics, 20, 1858-1864, 1981.

16. P.M. Charalambous et al., "Aberrations in Gamma-Ray Imaging Systems", Nucl. Instr. and Meth, A221, 56-59, 1984.

17. I.D. Jupp et al., "An Improved Sampling Configuration for a Coded Aperture Telescope", Nucl. Instrum. Meth., A345, 576-584, 1994.

18. F.P. Doty et al., "Properties of CdZnTe Crystals Grown by a High Pressure Bridgman Method", Journal of Vacuum Science and Technology, B10, 1418, 1992.

19. D.G. Marks et al., "A 48 × 48 CdZnTe Array with Multiplexer Readout", IEEE Trans. Nucl. Sci., 43, 1253-1259, 1996.

20. L.A. Hamel et al., "Signal Generation in CZT Strip Detectors", IEEE Trans. Nucl. Sci., 43, 1422-1426, 1996.

21. H.H. Barrett et al., "Charge Transport in Arrays of SEmiconductor Gamma-Ray Detectors", Phys. Rev. Lett. 75,156, 1995.

22. J.D. Eskin et al., "The Effect of Pixel Geometry on Spatial and Spectral Resolution in a CdZnTe Imaging Array", 1995 IEEE Nucl. Sci. Symp. Conf. Record, 1, 544-548, 1995.

23. V.V. Nagarkar et al., "Improved X-Ray Converters for CCD-Based Crystallography Detectors", SPIE Conf. Proc., 2519, 2-11, 1995.

24. N. Gehrels, "Instrumental Background in Balloon-Borne Gamma-Ray Spectrometers and Techniques for its Reduction", Nucl. Instr. and Meth., A239, 324-349, 1985.

25. R.C. Butler et al. , "An Evaluation of the Background Introduced from the Coded Aperture Mask in the Low Energy Gamma-ray Telescope Zebra", Nucl. Instr. and Meth., A221, 41-44, 1984.

26. J.E. Grindlay et al., "Energetic X-ray Imaging Survey Telescope (EXIST)", Bull. American Astronomical Soc., 27, 1386 (1995).

27. J.P. Roques, "Fast Decoding Algorithm for Uniformly Redundant Arrays", Applied Optics, 26, 3862-3865, 1987.

28. E.E. Fenimore, "Time-Resolved and Energy-Resolved Coded Aperture Images with URA-Tagging", Applied Optics, 26, 2760, 1987.

29. M.L. McConnell et al., "Gamma-Ray Observations of the Crab Region Using a Coded-Aperture Telescope", Ap.J., 321, 543-552, 1987.

30. Ph. Laudet and J.P. Roques, "Correction for Detector Uniformity of a Gamma-Ray Telescope Using Coded Aperture Imaging", Nucl. Instrum. Methods., A267, 212-217, 1988.

31. A.P. Hammersley and G.K. Skinner, Nucl. Instrum. Meth. 221, 45 (1984).

Downloaded From: http://proceedings.spiedigitallibrary.org/ on 11/25/2014 Terms of Use: http://spiedl.org/terms